Deng *et al.*
Journal of Engineering and Applied Science (2023) 70:135
https://doi.org/10.1186/s44147-023-00308-3

Journal of Engineering and Applied Science

RESEARCH Open Access

Evaluation of new target structure and recognition for point cloud registration and coordinates transformation of China's large double-span bridge

Xiaojun Deng[1*], Shaorui Wang[1,2], Yanghao Zhuang[1], Yonghui Fan[1] and Yin Zhou[1,2]

*Correspondence: 193125188@qq.com

[1] School of Civil Engineering, Chongqing Jiaotong University, Chongqing 400074, China
[2] State Key Laboratory of Mountain Bridge and Tunnel Engineering, Chongqing 400074, China

Abstract

In view of the limited precision of traditional point cloud registration methods in bridge engineering, as well as the lack of intuitive guidance for bridge construction control regarding relative coordinate relationships of point clouds, this study proposes a novel dual-purpose target for the total station and laser scanner, along with a corresponding algorithm. The scanning point cloud undergoes intensity filtering, clustering, planar denoising, contour extraction, centroid fitting, registration transformation, target recognition, registration, and coordinate transformation. Experimental results demonstrate that the proposed algorithm can accurately extract the centroid coordinates of the targets and effectively handle complex on-site conditions. The coordinate transformation achieves high precision, with an amplification error of only 2.1 mm at a distance of 500 m. The registration precision between planar and spherical targets is nearly identical, surpassing that of planar iterative and ICP algorithms. Application of the algorithm in the context of China's large double-span steel-tube concrete arch bridge scenario. it was found that the maximum deviation of the radius of the main chord tube was 10.8 mm, the maximum deviation of the distance from the center of the main chord tube was 8.3 mm, the average length of the merging opening was 775.0 mm, the maximum lateral deviation of the merging opening was 9.6 mm, and the maximum deviation of the height of merging opening was 25.2 mm. The results showed that no additional restraining measures were needed, and the smooth jointing could be realized only under a suitable temperature. Comparison with measurements obtained from the TS60 total station exhibits a close match, with a verification error within 3.9 mm, thereby meeting the precision requirements for construction control.

Keywords: Bridge engineering, 3D point cloud, Target design, Target recognition, Coordinate transformation, Construction control

Introduction

A three-dimensional laser scanner is a non-contact measurement tool used for rapidly acquiring surface topography data points [1]. Leveraging its advantages of high efficiency, sub-millimeter precision, safety, and high automation, three-dimensional scanning technology has been applied in bridge engineering for deformation monitoring, construction control, and digital twin applications [2]. In the case of large-scale scenes, the registration of multiple point clouds from ground-based three-dimensional laser scanners requires the selection of common points for stitching [3]. The iterative closest point (ICP) algorithm proposed by Besl [4] is considered the most classical registration algorithm to date. This algorithm achieves registration by iteratively finding the closest point pairs between point clouds. However, its applicability is limited in engineering scans due to the scarcity of overlapping points between stations. In recent years, scholars [5–7] have made improvements and researched this algorithm, proposing new algorithms that involve coarse registration followed by fine registration. These algorithms are commonly used in small-scale three-dimensional scans, where the precision is higher for experiments with small point cloud models such as Bunny, Elephant, and Horse from the Stanford database. In practical engineering applications, the large amount of point cloud data in large-scale scans can lead to long registration times, and the selection of registration iteration points becomes unknown, making it difficult to judge the algorithm's precision and its persuasive power. In comparison to algorithmic stitching methods, the manual selection of fixed points for stitching achieves higher precision, greater applicability, and better acceptance in engineering practices. Manual stitching includes automatic recognition of spherical targets and planar targets [8]. Wang Jun et al. [9] proposed that the stitching precision depends on the precision of extracting the sphere center and planar center of the spherical targets. Zhou [10] believed that factors such as high production cost, scarcity of point clouds at long distances, edge drift in target sphere point clouds, and difficulties in setting permanent observation points have resulted in the rare use of spherical targets in on-site construction control. The extensive post-processing time for large point cloud data necessitates the urgent need for a rapidly identifiable target to locate the spatial orientation of structures and provide timely feedback for adjustment during the construction process. Planar targets have emerged due to their advantages of simple production, low cost, high precision, and adjustable size.

Currently, domestic and international scholars have conducted comprehensive research on automated extraction methods for planar target point clouds. LICHTI et al. [11] proposed three automatic identification methods based on the assumption that the scan points with the highest reflectance intensity correspond to the center of the target. However, in reality, the center point does not always have the highest reflectance intensity, resulting in low identification precision. VALANIS et al. [12] proposed an automatic identification method using the fuzzy C-means clustering algorithm, but it cannot eliminate the influence of outliers and scanning noise. Zhou Shaoguang et al. [13] used the principle of central projection to project the point cloud data into a 2D image and employed the region-growing algorithm to fit the coordinates of the target center. Wang L et al. [14] utilized the reflectance intensity of the acquired point cloud data and applied a reflectance intensity-weighted approach to identify the center coordinates of the planar target. Chen JJ et al. [15]employed centroid-based and geometric-based methods to

obtain the coordinates of planar targets and analyzed and compared their accuracies. The results indicated that the geometric-based method yields better results when the point cloud distribution of the target is non-uniform, emphasizing the importance of acquiring good edge points of the target. Chen XJ et al. [16] divided the target point cloud into sections and calculated the mean clustering center of each section using the K-means algorithm as the target center coordinates. This algorithm mitigates the impact of missing data to some extent but cannot eliminate the influence of outliers. Zhu NN et al. [17] proposed an edge point fitting algorithm based on the geometric properties of the target, where the edge points are extracted by finding the farthest point for each point based on the point cloud distribution characteristics. The centroid coordinates are then calculated using the least squares method. This algorithm can handle the problem of incomplete target point clouds to some extent but cannot accurately calculate the centroid coordinates in the presence of redundant point clouds. Wu Chao et al. [18] employed the reflectance intensity values of the point cloud data for region segmentation. Based on the K-means clustering method applied to each segmented region, they determined the coordinates of the region's centroid, thereby obtaining the center coordinates of the planar target. However, this approach is unable to effectively eliminate the influence of outliers and noise. On the other hand, Fu YJ et al. [19] proposed an edge point extraction algorithm that selects the point farthest from the centroid of the target. They utilized robust least squares fitting to compute the centroid coordinates based on the extracted edge points. It should be noted that this algorithm is specifically suitable for circular targets with high reflectance rates.

The aforementioned algorithms have high requirements for planar targets, requiring them to be perfectly circular and have good flatness. Additionally, high reflectance intensity is needed, but excessively high reflectance intensity can damage the 3D laser scanner. While these algorithms demonstrate high precision in small-scale experiments, further research is needed to assess their applicability for precision construction control in large-scale bridge engineering scenarios. Inspired by previous studies, this paper combines the on-site construction conditions of a concrete-filled steel tubular (CFST) arch bridge to design a dual-purpose planar target for the total station and 3D scanner. Accompanied by corresponding identification and coordinate transformation algorithms, the aim is to achieve automated and rapid identification of targets and multi-station data registration for point cloud data in large-scale scenes. Experimental validation and application examples have been conducted to verify the precision and applicability of the proposed approach.

Methods

Target design methods

During the scanning process of bridge engineering and other large-scale scenes, the extensive volume of scan data often leads to prolonged post-processing time for point clouds. Consequently, real-time acquisition and positioning of structural spatial orientation become unattainable during construction and monitoring processes. This significantly hampers precise control during construction and timely feedback on monitoring data. Therefore, there is an urgent need to devise a specialized target and propose a rapid recognition algorithm to accurately extract the target from the vast point cloud data and

swiftly obtain high-precision target parameters. This enables the determination of structural spatial orientation and facilitates real-time monitoring of dynamic displacements in prefabricated component installation and control.

Traditional 3D scanning targets for registration between stations include stereoscopic targets and planar targets. Representative examples are spherical targets and black-and-white targets. Stereoscopic targets involve fitting feature points, such as the sphere center, using the point cloud on the target's surface. Black-and-white targets use the intersection points of black-and-white regions to register two or more stations through common points. However, spherical targets cannot quickly locate the sphere center using a total station, and the limited number of points on the sphere's surface and the fitting error result in significant inaccuracies. While black-and-white targets have clear intersection points, the use of non-prism measurements with a total station introduces large measurement errors, reducing confidence in coordinate transformation. As a result, these targets are generally not suitable for point cloud coordinate transformation. There is an urgent need to design a new type of high-precision scanning target that can be used for identification, registration, and coordinate transformation in both scanning and total station applications.

The new type of scanning target includes a target plate for direct aiming, a circular target disk, a prism lens, and a magnetic table base. Round target disk material for Polytetrafluoroethylene., and construction site materials reflective strength of the difference is very convenient for late data screening, cheap and easy to process, diameter of 200 mm, thickness of 5 mm, the center of the open 50×50 mm square hole used to place the Leica prism. Prism for the standard Leica round prism, lens diameter 25.4 mm, measuring distance of 800 m, precision of $5''$. The back of the comparison test shows that in a 50-m scanning distance, a single scanning round target point cloud number of about 2500, and precision can be guaranteed, in the case of scanning distance increases, should be increased accordingly the diameter of the round target, had a linear relationship. This new type of target serves as a dual-purpose target for both 3D scanning and total station applications. It features high precision, convenience, ease of use, and low cost. In addition, corresponding algorithms have been developed for rapid target recognition and feature point fitting. The algorithms also enable the conversion of relative coordinates to absolute coordinates for the point cloud, achieving full automation in the target recognition, conversion, and registration. The application scenarios for these targets are illustrated in Fig. 1.

Intensity screening methods

The point cloud data consists of three-dimensional coordinates (XYZ), intensity values (Intensity), and color information (RGB). The laser reflection intensity is the ratio of the reflected laser energy to the emitted laser energy. The intensity of reflection varies among different materials, colors, and angles. In the construction site of a steel-reinforced concrete arch bridge, the point cloud data mainly includes the ground, concrete structures, and steel components. In this experiment, a comparison and statistical analysis of the intensity values from the points on the target and the main objects in the scanning scene were conducted at different distances and incident angles. For each location, 1000 random points were selected for intensity statistics. Tests have proved that the

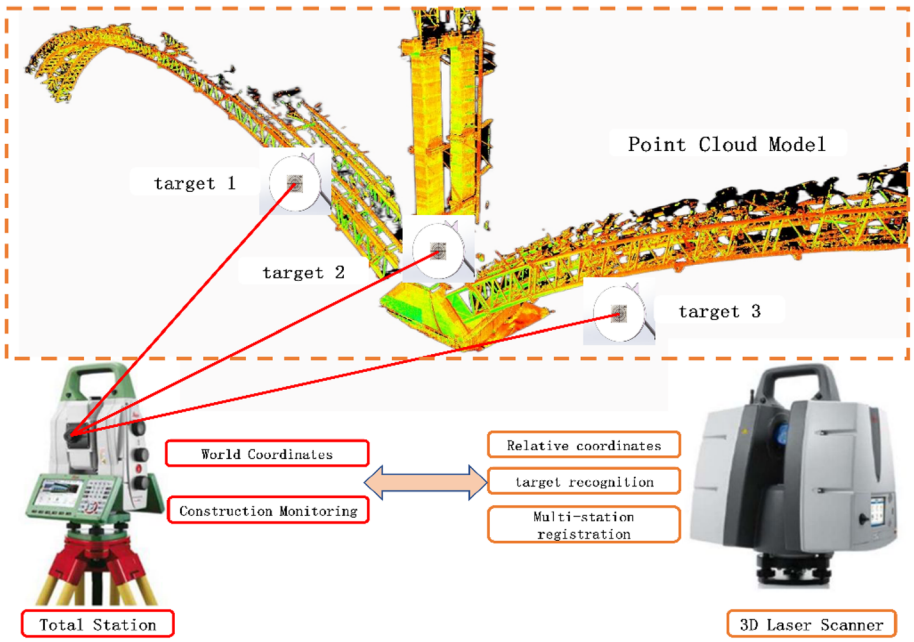

Fig. 1 Schematic diagram of target usage scenario

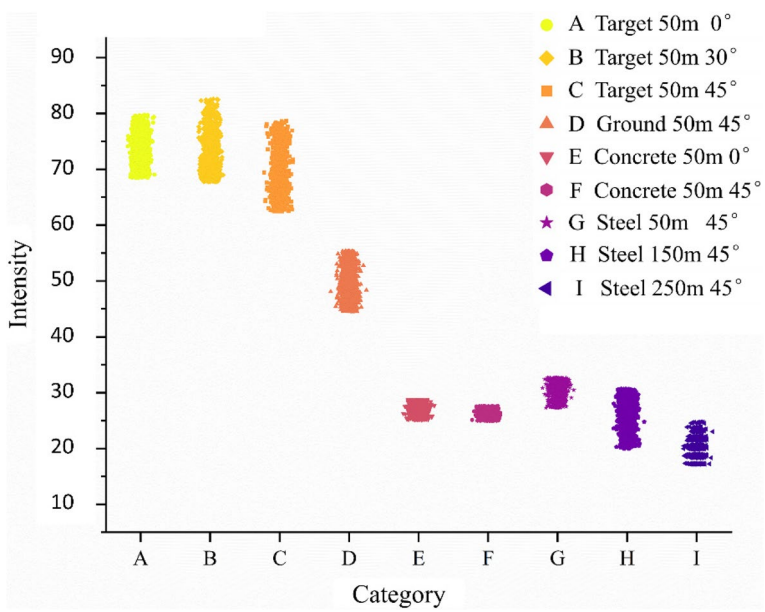

Fig. 2 Statistical distribution of intensity of different targets at different distances and angles

target should be facing the scanner that is, when the angle of incidence is 0°, the point intensity distribution of the target is more aggregated, and the distribution of the point cloud data is uniform to facilitate the algorithm for high-precision fitting, so when scanning, the target should be used to target the aiming device, rotating the magnetic pedestal and rotating the robotic arm to make the target and the scanner are facing each other. The statistical results are shown in Fig. 2, indicating that the intensity range of the target falls between 65 and 85 and does not overlap with the intensity ranges of other objects in

the field. By setting an appropriate intensity threshold, filtering and data mining can be performed.

Point cloud clustering methods

DBSCAN (density-based spatial clustering of applications with noise) is a typical density-based clustering algorithm [20]. It uses two parameters to describe the density of samples. The first parameter is the neighborhood radius, which represents the distance threshold for the current point's neighborhood. The second parameter is the minimum number of points required to form a dense region within the neighborhood. By setting appropriate values for the neighborhood radius and the number of points, the target point cloud can be separated from other point clouds. The principle of the DBSCAN algorithm is as follows:

1) Input sample set $\mathrm{D} = \{x_1 x_2 x_3 \ldots x_n\}$ and neighborhood parameter $\varepsilon, MinPts$;
2) Find core objects: if $N_\varepsilon(x_j) = \{x_i \in D | distance(x_i, x_j) \leq \varepsilon\}$ and $|N_\varepsilon(x_j)| \geq MinPts$, then x_j is a core point, x_j and the points x_j within its neighborhood belong to a new set Q_i;
3) In the remaining sample set D, identify other core points. If a new core object has sample points in its neighborhood belonging to set Q_i, then the core point and other sample points within its neighboring region all belong to set Q_i; otherwise, they belong to a new set Q_j;
4) Find all points in set D and obtain all clustering subsets $Q_1 Q_2 Q_3 \ldots Q_n$. If a point x_i does not belong to any new clustering subset, it is considered an outlier and is removed.

The processing principle and clustering results of the DBSCAN algorithm are shown in Fig. 3.

Plane fitting noise reduction methods

During the scanning process, atmospheric pressure and temperature can have an impact on the instrument, resulting in some points not being completely adhered to the object's surface. When the scanner reaches the edges of the object, large angles can cause distortion and drift in the reflected point cloud, collectively referred to as outliers. These outliers can introduce significant errors during subsequent target fitting, affecting registration and coordinate transformation. Therefore, it is necessary to eliminate points that

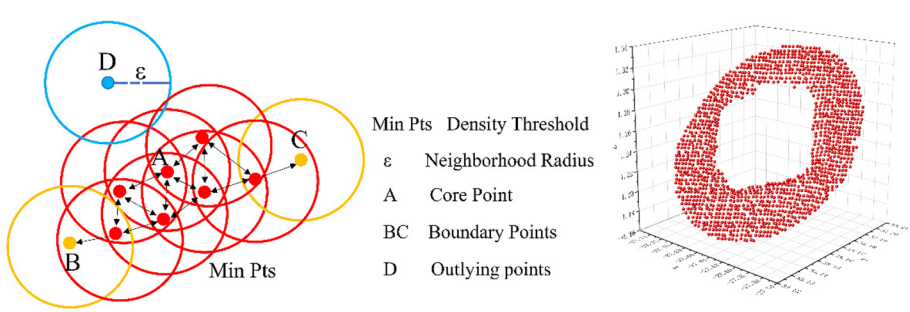

Fig. 3 DBSCAN schematic diagram and target clustering processing diagram

do not lie on the plane before performing the fitting process. The obtained fitted plane is optimal when the sum of squared distances from k nearest points to the plane is minimized, expressed as follows: The average coordinates of the point:

$$e = \sum_{i=1}^{n} d_i^2 \ \ min \tag{1}$$

where d_i is the distance from a point to the plane; e is the sum of the squares of the distances d_i from all points to the plane.

is represented as $(\overline{x}, \overline{y}, z)$, given by

$$a\overline{x} + b\overline{y} + c\overline{z} + d = 0 \tag{2}$$

$$a(x_i - \overline{x}) + b(\overline{y} - y) + c(z_i - \overline{z}) = 0 \tag{3}$$

$$A = \begin{bmatrix} x_1 - \overline{x} & y_1 - \overline{y} & z_1 - \overline{z} \\ x_2 - \overline{x} & y_2 - \overline{y} & z_2 - \overline{z} \\ x_3 - \overline{x} & y_3 - \overline{y} & z_3 - \overline{z} \\ & \cdots & \\ x_n - \overline{x} & y_n - \overline{y} & z_n - \overline{z} \end{bmatrix} X = \begin{bmatrix} a \\ b \\ c \end{bmatrix} \Rightarrow AX = 0 \tag{4}$$

In practical situations, some points lie outside the plane. The purpose of the fitting is to minimize the sum of distances between the plane and all points. To achieve this, matrix A is solved using singular value decomposition (SVD):

$$A = UDV^T \Rightarrow \|AX\| = \|UDV^T X\| = \|DV^T X\| \tag{5}$$

The minimum value of e corresponds to the minimum eigenvalue of matrix A, with the corresponding eigenvector representing the plane parameters a, b, and c. The value of d is obtained using the centroid. The error in the best-fit plane can be calculated as follows:

$$\delta = \sqrt{\frac{\sum_{i=1}^{n} d_i^2}{n}} \tag{6}$$

Remove points where $d_i > 2\delta$, iterate repeatedly until the difference between the errors of the previous and current iterations is less than 0.1 mm.

Based on Table 1 and Fig. 4, it can be observed that after 6 iterations, the number of noisy points in the planar target reduced by 1853 points, representing a reduction of 43.24% in outliers. The resulting error in the fitted plane is 0.5 mm, and the maximum distance from points to the plane is 1.0 mm, indicating a sub-millimeter level of precision. Therefore, it can be concluded that the remaining points are approximately located on the same plane.

Target localization methods

Given the coordinates of three or more points on a circular circumference, the center coordinates of the circle can be computed through the fitting. After selecting the

Table 1 Iterative noise reduction for target plane fitting

Iteration	*a*	*b*	*c*	RMSE δ (mm)	Points	d_{min}(mm)	d_{max}(mm)
0	0.7716	−0.5482	0.3226	2.2	4285	−10.9	6.0
1	0.7699	−0.5472	0.3283	1.2	3821	−3.1	3.0
2	0.7699	−0.5469	0.3289	1.0	3598	−2.0	2.0
3	0.7702	−0.5466	0.3287	0.8	3217	−1.6	1.6
4	0.7710	−0.5458	0.3279	0.7	2871	−1.2	1.2
5	0.7719	−0.5448	0.3276	0.6	2574	−1.1	1.1
6	0.7726	−0.5443	0.3267	0.5	2432	−1.0	1.0

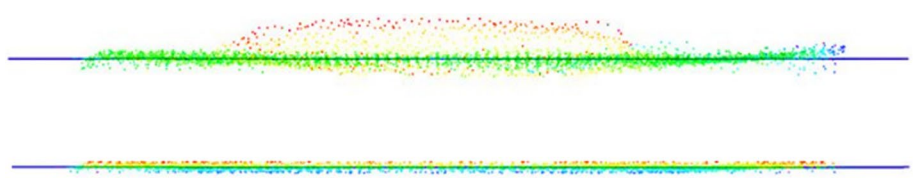

Fig. 4 The original point cloud of the target plane and the point cloud after 6 iterations

points on the planar surface, the point cloud becomes a spatial planar point cloud. Firstly, the spatial planar point cloud is projected onto the coordinate system of the best-fit plane. Secondly, the convex hull algorithm is applied to extract the outer contour of the target. Then, an iterative least squares method is used to filter out points with significant contour errors. Finally, the center coordinates of the circle and the parameters of the target are computed.

1. Projection is performed to rotate the best-fit plane parallel to the XOY plane, facilitating the fitting of the circle center:

$$\begin{cases} x_{i0} = x_i - a\left(ax_i + by_i + cz_i + d\right) \\ y_{i0} = y_i - b\left(ax_{i0} + by_i + cz_i + d\right) \\ z_{i0} = z_i - c\left(ax_{i0} + by_i + cz_i + d\right) \end{cases} \tag{7}$$

In the equation, $\left(x_{i0}, y_{i0}, z_{i0}\right)$ represents the projected plane coordinates, and (x_i, y_i, z_i) represents the coordinates of the target.

The rotation matrix is:

$$R = R_x R_y = \begin{bmatrix} cos\beta & 0 & -sin\beta \\ 0 & 1 & 0 \\ sin\beta & 0 & cos\beta \end{bmatrix} \begin{bmatrix} 1 & 0 & 0 \\ 0 & cos\alpha & sin\alpha \\ 0 & -sin\alpha & cos\alpha \end{bmatrix} \tag{8}$$

where α represents the angle between the plane normal vector and the Z-axis projection in the YOZ coordinate system, and β represents the angle between the plane normal vector and the Z-axis projection in the XOZ coordinate system. $cos\alpha sin\alpha cos\beta sin\beta$ can all be determined from the plane normal vector.

2. The convex hull algorithm Liu K et al. [21] is employed to find the minimum polygon that surrounds all the points on the plane, which represents the outer contour of the point cloud on the plane. The algorithm follows these principles:

   1) Locate the point P with the minimum Y value among N points.
   2) Sort the remaining points counterclockwise based on their distances and angles relative to point P.
   3) Starting from point P, connect the points counterclockwise, discarding any point that forms a concave shape until a convex shape is closed.
   4) Iterative least squares method is used to calculate the coordinates of the circle center and the parameters of the target.

The principle of least squares circle curve fitting is applied.

$$r^2 = (x - A)^2 + \left(y - B\right)^2 \tag{9}$$

The squared difference of the radius of the distance between the center of the circle and the point cloud is

$$\delta_i = d_i^2 - r^2 = (X_i - A)^2 + (Y_i - B)^2 - r^2 = X_i^2 + Y_i^2 + aX_i + bY_i + c \tag{10}$$

Let $Q(a, b, c)$ be the sum of the squares of δ_i, that is:

$$Q(a, b, c) = \sum \delta_i{}^2 = \sum \left(X_i^2 + Y_i^2 + aX_i + bY_i + c\right)^2 \tag{11}$$

The partial derivatives are computed to solve for a, b, c. By finding the value of a that minimizes the Q value, we can determine the circle fitted using the least squares method. The radius (r) and the coordinates of the center (A, B) are obtained through this process. The root mean square error (RMSE) of each point to the center of the circle is then calculated.

$$\sigma = \sqrt{\frac{1}{N} \sum_{i=1}^{N} (X_i - A)^2 + (Y_i - B)^2 - r^2)} \tag{12}$$

The absolute difference between the distances (d_i) from each point to the center of the circle and the fitted radius (r) is calculated. If the difference is greater than 2σ, the point is discarded; if it is smaller than 2σ, the point is retained. This process continues iteratively until the absolute difference between the fitted radii of two consecutive iterations is less than 0.1 mm.

3. The obtained coordinates of the center of the circle are transformed back to the spatial coordinates (XYZ) using inverse rotation operations

As shown in Table 2 and Fig. 5, after 3 iterations, the plane target experienced a reduction of 60 outliers, accounting for a decrease of 30.92% in gross errors. The resulting plane fitting error is 0.7 mm, and the maximum distance from points to the circular arc is 1.1 mm. The absolute difference in fitted radii between consecutive

Table 2 Iterative noise reduction table for target bullseye fitting

Iteration	x(m)	y(m)	z(m)	r(mm)	RMSEδ(mm)	Points	$d_{min} - r$(mm)	$d_{max} - r$(mm)
0	− 2.1630	46.6644	− 0.2361	95.6	1.2	194	-1.4	1.4
1	− 2.1630	46.6645	− 0.2361	95.6	1.0	177	-1.3	1.3
2	− 2.1632	46.6643	− 0.2361	95.6	0.8	154	-1.1	1.2
3	− 2.1633	46.6642	− 0.2360	95.6	0.7	134	-1.0	1.1

Fig. 5 Original and 3-iteration point cloud of the convex package contour of target

iterations is 0.1 mm, indicating that the remaining points are approximately located on the same circle. Therefore, the fitted circle exhibits a high level of precision in terms of the precision of the obtained center.

Coordinate conversion methods

The coordinate transformation between two coordinate systems, assuming consistent scaling ratios in all directions, can be represented by seven parameters: three rotation parameters, three translation parameters, and one scale parameter. Ou H-P et al. [22] Given the coordinates of three points in both coordinate systems A and B, these seven parameters can be uniquely determined. In point cloud models, where there is no scaling parameter other than 1, theoretically, only two points are needed to complete the coordinate transformation.

The mathematical model for coordinate transformation is as follows:

$$\begin{bmatrix} X \\ Y \\ Z \end{bmatrix}_A = \lambda \left(\begin{bmatrix} \Delta X \\ \Delta Y \\ \Delta Z \end{bmatrix} + R \begin{bmatrix} X \\ Y \\ Z \end{bmatrix}_B \right) \tag{13}$$

where λ is the scaling parameter set to 1, R represents the rotation matrix, Δ is the translation vector, and A and B represent coordinates in two different coordinate systems. The rotation matrix R is constructed using the skew-symmetric matrix S, where I denote the identity matrix.

$$S = \begin{bmatrix} 0 & -c & -b \\ c & 0 & -a \\ b & a & 0 \end{bmatrix} R = \frac{I+S}{I-S} \tag{14}$$

$$\begin{bmatrix} a \\ b \\ c \end{bmatrix} = \begin{bmatrix} 0 & -(\lambda Z_{B12} + Z_{A12}) & -(\lambda Y_{B12} + Y_{A12}) \\ -(\lambda Z_{B12} + Z_{A12}) & 0 & (\lambda X_{B12} + X_{A12}) \\ (\lambda Y_{B13} + Y_{A13}) & (\lambda X_{B13} + X_{A13}) & 0 \end{bmatrix}^{-1} \begin{bmatrix} X_{A12} - \lambda X_{B12} \\ Y_{A12} - \lambda Y_{B12} \\ Z_{A13} - \lambda Z_{B13} \end{bmatrix} \tag{15}$$

Results

Experimental scanning was conducted on a specially designed target in a large-scale scene. The scanning background was the 9th pier of a concrete-filled steel tubular arch bridge, using the Leica Scan Station P50 scanner. The scanning resolution was set at 3.1 mm@10 m, and the densification resolution was 1.6 mm@10 m. The scanning distance covered was 270 m, with two scanning stations, and each station required 14 min and 36 s. The target was positioned at a distance of 50 m from the scanner. The total station used was the Leica Nova TS60, with a prism precision of 0.6 + 1 ppm and a non-prism measurement precision of 2 mm + 2 ppm. The coordinate system employed was based on the construction control network of the CFST arch bridge. The target was positioned at a distance of 80 m from the total station. The layout of the experimental scene is illustrated in Fig. 6.

Target recognition precision result

Coordinate conversion precision result

During the relative coordinate transformation to world coordinates, when the lengths of line segments between two points are not consistent, forced displacement and rotation occur in the coordinate transformation. This forced displacement and rotation result in transformation errors and registration errors, which linearly amplify with increasing distance. In this study, Leica TS60 total station was used to measure the target center and the identified target center for coordinate transformation, and the precision of the transformation and registration was analyzed. The measurement results are presented in Table 3.

Alignment precision result

In bridge engineering, point cloud data registration between multiple stations is commonly achieved through methods such as plane target registration, spherical target registration, iterative registration using feature planes, and ICP (iterative closest point) algorithm registration (a reference to literature). In this case, the target mentioned above was used for two-station point cloud data registration, and a comparative analysis was conducted with other methods. The pre- and post-registration point cloud poses can be seen in Figs. 7 and 8, respectively.

Fig. 6 Test site layout scene

Table 3 Total station and scanner measurement results

	Leica Nova TS60 measurements			Algorithm of this paper		
Target number	*x*(m)	*y*(m)	*z*(m)	*x*(m)	*y*(m)	*z*(m)
1	95,866.7223	− 12.6926	492.6047	− 2.1633	46.6642	− 0.2360
2	95,886.2099	− 3.3242	495.1441	− 22.0447	55.1666	2.3041
3	95,866.6934	16.3879	492.6237	− 24.0349	27.4989	− 0.2163

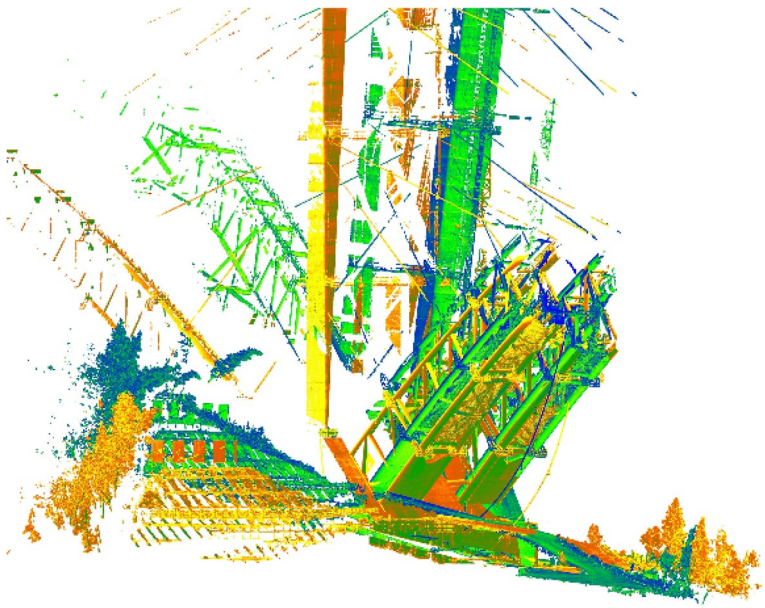

Fig. 7 Pre-registration attitude

Discussion

According to the comparison table in Tables 4 and 5, which compares the parameters of the proposed algorithm, the algorithm from Fu YJ, and the centroid method for target recognition, it can be observed that in comparison to the centroid method, the proposed algorithm exhibits a maximum positional difference of 0.6 mm in the coordinate components and an average absolute difference of 0.4 mm in the coordinate components. The errors are within the sub-millimeter range. These errors are attributed to the presence of highly reflective stickers on the center of the target, which cause point cloud drift near the center and affect the precision of the centroid method. In comparison to the algorithm in Fu YJ's, the proposed algorithm shows a maximum positional difference of 0.1 mm in the coordinate components and an average absolute difference of 0.1 mm in the coordinate components. The coordinates of the target center are nearly identical, indicating that the proposed algorithm achieves a comparable level of precision to that of the referenced algorithm.

When comparing the four sets of point cloud data containing initial defects, the precision of the centroid method significantly decreases with an increase in the unevenly distributed defects. For instance, when two-thirds of the target is occluded, the positional differences in the coordinate components using the centroid method are

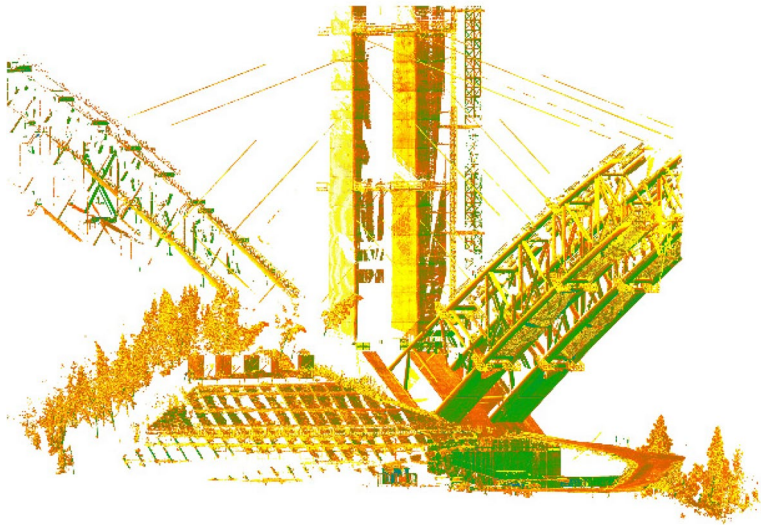

Fig. 8 Post-registration effect

Table 4 Comparison of target identification between the algorithm of this paper and Fu YJ's

		Algorithm of this paper			Fu YJ 's			Difference value (mm)		
Number	**Feature**	*x*(m)	*y*(m)	*z*(m)	*x*(m)	*y*(m)	*z*(m)	Δ*x*	Δ*y*	Δ*z*
1	Full	− 2.1633	46.6642	− 0.2360	− 2.1632	46.6643	− 0.2361	− 0.1	0.0	0.0
	Defects1/3	− 2.1633	46.6642	− 0.2361	− 2.1632	46.6642	0.2360	− 0.1	0.0	0.0
	Defects2/3	− 2.1632	46.6643	− 0.2359	− 2.1633	46.6642	− 0.2360	0.1	0.1	0.1
	Cover 1/3	− 2.1629	46.6634	− 0.2360	− 2.1631	46.6632	− 0.2362	0.2	0.2	0.2
	Cover 2/3	− 2.1630	46.6626	− 0.2367	− 2.1632	46.6625	− 0.2369	0.2	0.1	0.2
2	Full	− 22.0447	55.1666	2.3041	− 22.0446	55.1666	2.3040	− 0.1	0.0	0.0
3	Full	− 24.0349	27.4989	− 0.2163	− 24.0349	27.4989	− 0.2163	0.0	0.0	0.0

11.1 mm, 34.4 mm, and 55.9 mm, respectively. In contrast, the proposed algorithm yields positional differences in the coordinate components of 0.3 mm, − 0.6 mm, and − 0.6 mm, while the algorithm in Fu YJ's yields positional differences of 0.1 mm, − 0.7 mm, and − 0.8 mm. These errors are within the sub-millimeter range. It can be concluded that the proposed algorithm can effectively adapt to sudden situations such as occlusions and target defects in the field, demonstrating its strong applicability.

Based on Table 6, which shows the coordinate transformation results and the coordinate differences, it can be observed that the maximum point-wise difference in coordinate components after the transformation of the 50-m target is 0.2 mm. The absolute average coordinate component difference is 0.1 mm. By linearly amplifying the displacement error based on the maximum point displacement deviation, the errors at distances of 100 m, 200 m, 300 m, 400 m, and 500 m are 0.4 mm, 0.8 mm, 1.2 mm, 1.7 mm, and 2.1 mm, respectively. These dual-purpose targets are capable of meeting the coordinated transformation and registration requirements for kilometer-scale bridges.

Table 5 Comparison of target identification between the algorithm of this paper and the center-of-centroid method

Number	Feature	Algorithm of this paper (m)			the center-of-centroid method			Difference value (mm)		
		x(m)	y(m)	z(m)	x(m)	y(m)	z(m)	Δx	Δy	Δz
1	Full	−2.1633	46.6642	−0.2360	−2.1629	46.6638	−0.2365	−0.3	0.5	0.5
	Defects1/3	−2.1633	46.6642	−0.2361	−2.1651	46.6653	−0.2282	1.8	−1.0	−7.8
	Defects2/3	−2.1632	46.6643	−0.2359	−2.1685	46.6651	−0.2214	5.3	−0.7	−14.5
	Cover 1/3	−2.1629	46.6634	−0.2360	−2.1494	46.6840	−0.2181	−13.5	−20.6	−17.9
	Cover 2/3	−2.1630	46.6626	−0.2367	−2.1519	46.6981	−0.1806	−11.2	−35.5	−56.1
2	Full	−22.0447	55.1666	2.3041	−22.0443	55.1660	2.3043	−0.4	0.6	−0.3
3	Full	−24.0349	27.4989	−0.2163	−24.0347	27.4985	−0.2167	−0.2	0.4	0.3

Table 6 Coordinate conversion results and differences

Target number	x(m)	y(m)	z(m)	Δx(mm)	Δy(mm)	Δz(mm)
1	95,866.7221	−12.6927	492.6044	0.1	0.0	0.2
2	95,886.2100	−3.3242	495.1442	−0.1	−0.1	−0.1
3	95,866.6934	16.3879	492.6238	0.0	0.0	−0.1

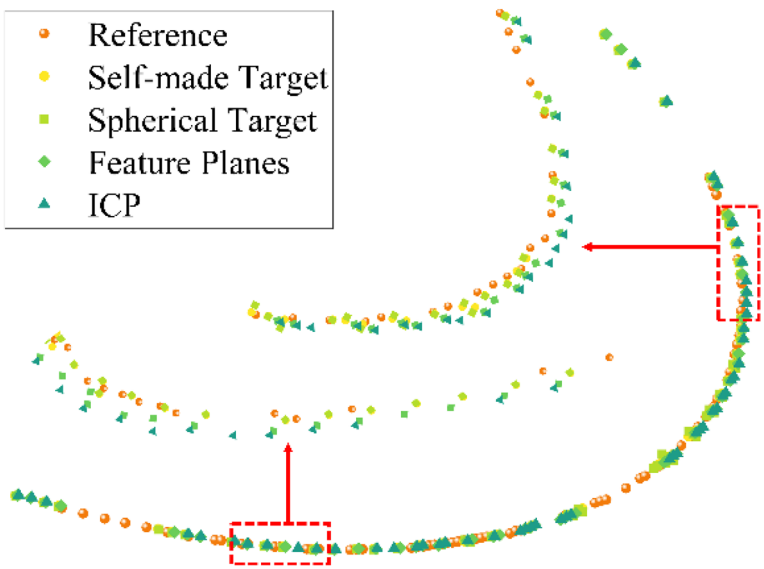

Fig. 9 Steel tube arch rib registration difference

From the partial registration results shown in Figs. 9 and 10, it can be observed that on the arch plane, the precision of various methods is comparable. Both the iterative registration using feature planes and the ICP algorithm show high precision, with an RMS (root mean square) error of 1.5 mm for ICP point cloud registration. This is because both the iterative registration using feature planes and the ICP algorithm are based on the reference of the plane for iterative registration. On the steel arch ribs, the registration results of the plane target and the spherical target are almost identical, and their registration precision is better than that of the iterative registration using feature planes and the ICP algorithm. However, the feature plane iterative registration and the ICP algorithm show smaller errors on the ground of the arch rib compared to the errors on the side of the arch rib. This is because the algorithm achieves high precision in recognizing the central coordinate parameters of the target, resulting in smaller forced displacements and less obvious point cloud layering after registration. The feature plane iterative registration relies on the presence of large fixed plane objects in the field, such as the arch in this experiment, to achieve higher precision. However, if there are no distinct feature planes, such as in the scanning of the north and south banks of a steel arch bridge where the overlap is only a small part of the curved tube at the mid-span position, the registration error will be significant. The ICP algorithm relies on the overlap degree and initial pose of the two-station

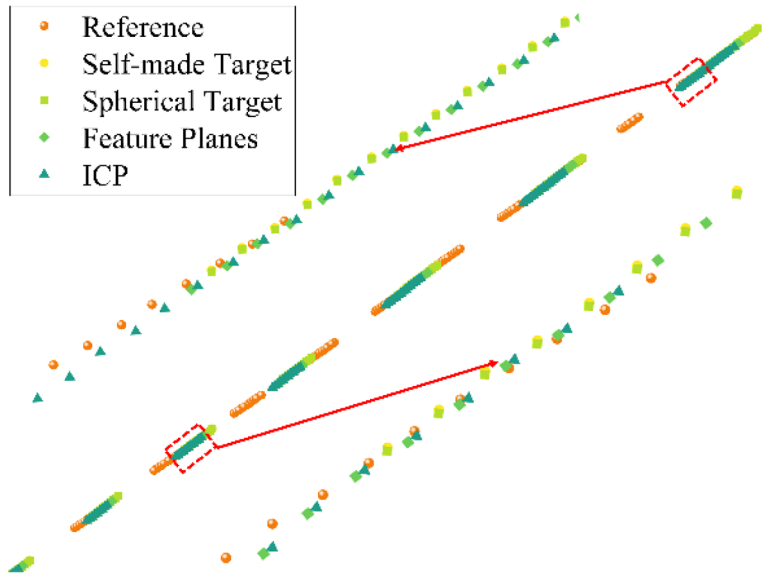

Fig. 10 Arch seat plane registration difference

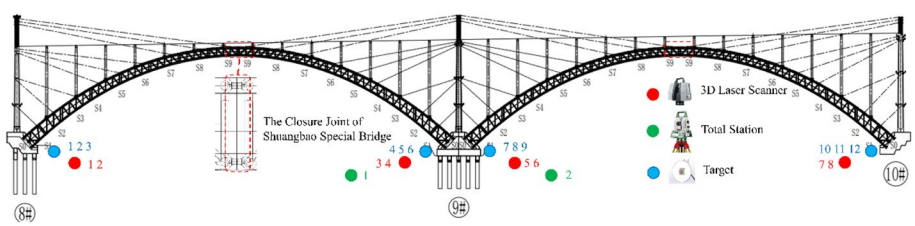

Fig. 11 Scanning layout and target location schematic

point clouds. In bridge engineering, where scanning is typically performed in large-scale scenes with low overlap between two stations, the ICP algorithm often fails to converge and exhibits large registration errors. Based on the above analysis, it can be concluded that the plane target can meet the registration precision requirements and is suitable for the fast registration of multi-station data.

Application examples

Here is one of the world's largest double-span continuous arch bridges, with a main span of 2×405 m. It is symmetrically arranged with two spans and is also the first project in China to fully apply three-dimensional laser scanning and digital pre-assembly technology. The closure of the arch bridge is the most important construction milestone, and for the CFST arch bridge, the closure involves both spans simultaneously. In the state of the large cantilever, all four arch ribs are closed simultaneously, with four main tie bars for each rib, totaling 16 working faces. The closure requires extremely high precision in terms of elevation and alignment at the end points Fig. 11.

To achieve precise closure of the main arch, three-dimensional laser scanning technology is used to detect the closure joint, measuring its elevation, alignment, and deviation. To test the measurement precision, coordinate measurements of the

Fig. 12 Multi-station registration point cloud of the CFST arch bridge (2 × 400 m)

Table 7 Scanner measurement of the center coordinates of the chord pipe at the end of the joint

Parts	Mileage	*x* (m)	*y* (m)	*z* (m)	*r* (mm)
2# Lower left-hand string	Little	96,050.1064	4.9848	576.6385	701.7
	Large	96,050.8838	4.9944	576.6166	689.2
2# Lower right-hand string	Little	96,050.1054	12.4932	576.6435	701.7
	Large	96,050.8829	12.5005	576.6244	689.2
2# Higher right-hand string	Little	96,050.1082	12.4902	583.1681	701.7
	Large	96,050.8845	12.4959	583.1468	689.2
1# Lower left-hand string	Little	95,645.1144	4.9945	576.6263	700.4
	Large	95,645.8835	4.9987	576.6305	691.5
1# Lower right-hand string	Little	95,645.1162	12.4979	576.6329	711.6
	Large	95,645.8814	12.5015	576.6453	698.4
1# Higher right-hand string	Little	95,645.1110	12.4962	583.1582	706.4
	Large	95,645.8921	12.4996	583.1672	696.4

sample points are also conducted using a total station for precision verification. Due to size limitations, the scanning covers two lower chord tubes and the outermost upper chord tube of the right side of arch ribs 1 and 2. The total station is used to measure the sample points on the outermost upper chord tube of the right side of arch ribs 1 and 2, with the sample points located 10 cm away from the segment ends. The point cloud model of the CFST is shown in Fig. 12.

According to Table 7, which presents the measured center coordinates of the closure joint's chord tube using the scanner, the theoretical radius of the main chord tube for the CFST arch bridge is 700 mm. The center distance between the left and right main chord tubes is 7500 mm, and the center distance between the upper and lower main chord tubes is 6500 mm. After conducting three-dimensional laser scanning to inspect the closure joint, the average radius of the chord tube is measured to be 698.1 mm. The center distances between the left and right chord tubes are measured to be 7508.3 mm, 7506.1 mm, 7503.4 mm, and 7502.9 mm, while the center distances between the upper and lower chord tubes are measured to be 6524.6 mm, 6522.3 mm, 6525.3 mm, and 6521.9 mm, slightly larger than the theoretical values. The discrepancy in measurements is attributed to the deformations caused by the self-weight of the segments, which is around 200 tons, and the tensions of approximately 100 tons generated during the tensioning process. These factors result in slight variations in the measurements. The reliable measurement precision of the three-dimensional scanning results indirectly demonstrates the precision and reliability of the scanning technique.

According to Table 8, which provides the results of the closure joint inspection using the scanner and the total station, it is evident that there is a significant height difference in the right section of the 2nd arch rib. This is attributed to the construction sequence of the CFST arch bridge, where the 2nd arch rib was initially lifted. During the lifting of the 9th segment, only 80% of the theoretical tensioning force was applied, leaving a 20% reserve force to adjust the elevation of the closure joint. The theoretical length of the closure joint for the CFST arch bridge is 798 mm, but the measured result is 775.0 mm. This discrepancy can be attributed to the measurement being conducted in the afternoon when the temperature was relatively high. The elevated temperature caused deformations in the arch rib, resulting in a decrease in elevation and an increase in length. It was found that the maximum lateral deviation of the merging opening was 9.6 mm, and the maximum deviation of the height of the merging opening was 25.2 mm. The results showed that no additional restraining measures were needed, and the smooth jointing could be realized only under a suitable temperature. The pattern of the measurement data obtained from the total station aligns with this observation, with the maximum discrepancy of 3.9 mm occurring in the elevation dimension.

Conclusions

The proposed combined total station and scanner with the corresponding planar target, as well as the introduced recognition, registration, and transformation algorithm, enable efficient and precision extraction of the target center coordinates and can handle complex on-site conditions. The precision of target recognition can reach the sub-millimeter level. The coordinate transformation achieves high precision, with an error amplification of 2.1 mm at a distance of 500 m, meeting the requirements for kilometer-level bridge coordinate transformation precision. The alignment precision between the planar target and the spherical target is nearly identical and higher than that of the feature plane iterative registration and ICP algorithm, satisfying the alignment precision requirements. This approach is suitable for the fast registration of multi-station point cloud data. Application of the algorithm in the context of China's large double-span steel-tube concrete arch bridge scenario. it was found that the maximum deviation of the radius of the main chord tube was 10.8 mm, the maximum deviation of the distance from the center of the main chord tube was 8.3 mm, the average length of the merging opening was 775.0 mm, the maximum lateral deviation of the merging opening was 9.6 mm, and the maximum

Table 8 Scanner and total station merging port inspection

Arch ribs	Parts	Length Combination (mm)	Y-Off-set (mm)	H-difference (mm)
2# Arch rib right	Lower left	777.4	9.6	21.9
	Lower right	777.5	7.3	19.1
	Scanners Higher R	776.3	5.6	21.3
	Total stations H-R	776.7	6.4	25.2
1# Arch rib right	Lower left	769.2	4.1	-4.1
	Lower right	765.1	3.6	-12.5
	Scanners Higher-R	781.1	3.5	-9.0
	Total stations H-R	776.5	5.5	-5.3

deviation of the height of merging opening was 25.2 mm. The results showed that no additional restraining measures were needed, and the smooth jointing could be realized only under a suitable temperature. The results obtained using the Leica Nova TS60 total station on-site measurement are almost consistent with the proposed method, with a maximum verification error of 3.9 mm. This indicates that the proposed approach can meet the precision requirements for construction control and effectively guide on-site construction with high efficiency and quality.

Abbreviations

RGB	Red, green, blue
DBSCAN	Density-based spatial clustering of applications with noise
SVD	Singular value decomposition
RMSE	Root mean square error
ICP	Iterative closest point
CFST	Concrete-filled steel tube

Acknowledgements
The authors would like to thank the School of Civil Engineering, Chongqing Jiaotong University, and the State Key Laboratory of Mountain Bridge and Tunnel Engineering for providing a Leica Scan Station P50 3D laser scanner for this study.

Authors' contributions
Xiaojun Deng participated in all phases of the study, including modeling, formulation analyzing, and interpreting the results. Shaorui Wang developed the research methodology. Yanghao Zhuang, Yonghui Fan, and Yin Zhou participated in field trials and case validation. All authors have read and approved the manuscript.

Funding
Chongqing Natural Science Foundation (cstc2021jcyj-msxm2491); Chongqing Science and Technology Bureau (CSTB0TIAD-KPX0205); Chongqing Municipal Education Commission, "Construction of Twin Cities Economic Circle in Chengdu-Chongqing Region" Science and Technology Innovation Project (KJCXZD2020032); Guangxi Key R&D Program (Gui Ke AB22036007-8).

Availability of data and materials
The datasets used and/or analyzed during the current study are available from the corresponding author upon reason-able request.

Declarations

Competing interests
The authors declare that they have no competing interests.

Received: 30 August 2023 Accepted: 24 October 2023
Published online: 11 November 2023

References

1. Hosamo HH, Hosamo MH (2022) Digital twin technology for bridge maintenance using 3D laser scanning: a review advances in civil engineering. 1–15. https://doi.org/10.1155/2022/2194949.
2. Rashidi M, Mohammadi M, Sadeghlou Kivi S, Abdolvand MM, Truong-Hong L, Samali B (2020) A decade of modern bridge monitoring using terrestrial laser scanning: review and future directions. Remote Sensing 12: 37–96. https://doi.org/10.3390/rs12223796.
3. Chen H, Wang YB, Huang HP (2023) A multi-station 3D point cloud alignment method for non-spherical targets based on streamline clustering. Adv Laser Optoelectron 1–15. https://kns.cnki.net/kcms/detail/31.1690.TN.20221121.0939.014.html.
4. Besl PJ, McKay HD (1992) A method for registration of 3-D shapes. IEEE Trans Pattern Anal Mach Intell 14(2):239–256. https://doi.org/10.1109/34.121791
5. Ji S, Ren Y, Ji Z, Liu X, Hong G (2017) An improved method for registration of point cloud. Optik 140:451–458. https://doi.org/10.1016/j.ijleo.2017.01.041
6. Sahillioğlu Y, Kavan L (2021) Scale-Adaptive ICP. Graph Models 116:101–113. https://doi.org/10.1016/J.GMOD.2021.101113
7. Guo Y, Zhao L, Shi Y, Zhang X, Du S, Wang F (2022) Adaptive weighted robust iterative closest point. Neurocomputing 508:225–241. https://doi.org/10.1016/J.NEUCOM.2022.08.047
8. Zhao CC, Wang N, Li JB et al (2021) Research on the precision of spherical target recognition by ground laser scanne. Engineering Survey 49(09):55–59

9. Wang J, Li Z (2020) Analysis of point cloud splicing precision and mapping of ancient buildings. Eng Survey 48(02):73–78
10. Zhou Y (2021) Research on digital twin method of bridge structure and its application in condition inspection and performance evaluatio. Chongqing Jiaotong Univ. https://doi.org/10.27671/d.cnki.gcjtc.2021.001100
11. Lichti DD, Stewart MP, Tsakiri M et al (2000) Benchmark tests on a three-dimensional laser scanning system. Geomat Res Australas 72:1–24
12. Valanis A, Tsakiri M (2004) Automatic target identification for laser scanners. International Society for Photogrammetry and Remote Sensing, Istanbul, pp 1–7
13. Zhou S, Tian H, Li H (2012) Automatic implementation of extracting planar targets and aligning point clouds. Eng Surv 40(02):66–69
14. Wang L, Li GY, Zhang HX (2011) Automatic identification of planar targets based on return light intensity. Infrared Laser Eng 40(10):1910–1913
15. Chen JJ, Yan WT (2011) Research on the extraction method of center coordinates of plane targets based on laser point cloud. Eng Survey 8:53–57
16. Chen XJ, Hua XH, Yang RH et al (2013) Planar target localization by banded K-means clustering. J Wuhan Univ Inform Sci 38(2):167–170. https://doi.org/10.13203/j.whugis2013.02.011
17. Zhu NN, Lu S, Li XY (2014) A planar bull's-eye extraction algorithm. Geodesy Geodynamics 34(3):173–178. https://doi.org/10.14075/j.jgg.2014.03.041
18. Wu C, Yuan Y, Zhang M (2015) Study of planar target localization based on reflection intensity and K-means clustering. Laser Technol 39(3):341–344
19. Fu YJ, Li ZC, He H (2018) Robust bullseye positioning algorithm for retroreflective planes. J Geoinform Sci 20(4):422–429
20. Yiting L ,Lei Z ,Peijuan L, et al (2023) Laser radar data registration algorithm based on DBSCAN clustering. Electronics 12(6). https://doi.org/10.3390/ELECTRONICS12061373.
21. Liu K, Xia M, Yang X (2017) An efficient convex wrapping algorithm for planar point sets. Eng Sci Technol 49(05):109–116. https://doi.org/10.15961/j.jsuese.201601149
22. Ou H-P, Lv C-G, Yu Y-P et al (2019) The transformation method of two sets of Gaussian plane coordinates with different ellipsoidal and projection parameters. Survey Mapping Eng 28(01):1–4. https://doi.org/10.19349/j.cnki.issn1006-7949.2019.01.001

Publisher's Note

Springer Nature remains neutral with regard to jurisdictional claims in published maps and institutional affiliations.